RSC Advances

ROYAL SOCIETY OF CHEMISTRY

www.rsc.org/advances

Cite this: DOI: 10.1039/c0xx00000x

www.rsc.org/xxxxxx

ARTICLE TYPE

Citrate modified ferrihydrite microstructure: Facile synthesis, strong adsorption and excellent Fenton-like catalytic properties

Xuhong Zhang,[a,b] Yanzhuo Chen,[a] Ning Zhao,[b] Hui Liu,[a,c] Yu Wei,*[a,c]

Received (in XXX, XXX) Xth XXXXXXXXX 20XX, Accepted Xth XXXXXXXXX 20XX

DOI: 10.1039/b000000x

Hierarchical citrate modified ferrihydrite microstructures (Fh1) with flower-like morphologies were successfully synthesized via a simple aqueous solution route without the addition of any organic solvent or surfactant. The obtained products were characterized by field emission scanning electron microscope (FESEM), high resolution transmission electron microscopy (HRTEM), X-ray diffraction (XRD), BET analyses, Fourier-transform IR spectroscopy (FTIR) and X-ray photoelectron spectroscopy (XPS). The prepared citrate modified ferrihydrite microstructures (Fh1) exhibited superior adsorption abilities for removal of methylene blue (MB) and Cr(VI) ions from aqueous solution. In addition, these citrate modified ferrihydrite microstructures also exhibited high activity to produce hydroxyl radicals through catalytic decomposition of H_2O_2 and could degrade highly concentrated MB solution at neutral pH. The results indicate that citrate modified ferrihydrite microstructures are very promising adsorbents and (photo-) Fenton-like catalysts for the treatment of pollutants.

1. Introduction

Iron oxide nanomaterials are promising for removing toxic heavy metal ions and organic pollutants from waste water, due to their low cost, natural abundance, strong adsorption capacity, easy separation, enhanced stability and environment-friendly properties.[1-13] Current applications of iron oxide nanomaterials in contaminated water treatment can be largely divided into three groups: (a) adsorbent for efficient removal of pollutants from the contaminated water. [14-18] (b) photocatalysts to break down or to convert contaminants into a less toxic form. [19-27] (c) heterogeneous Fenton catalyst for the treatment of pollutants. [28-31] It is strongly desirable to synthesize a novel iron oxide nanostructure that shows not only a fairly good adsorption capacity but also a heterogeneous Fenton and photo catalysis capability under visible illumination.

Ferrihydrite is a common, naturally occurring Fe(III) hydroxide in the earth's crust, soils and sediments. It plays a substantial role in the sequestration of contaminants from groundwater and streams through adsorption and co-precipitation due to its high surface area and intrinsic reactivity. When ferrihydrite is used as heterogeneous Fenton catalyst, the high surface area of ferrihydrite results in more contact between the catalyst, the H_2O_2 and the contaminant, thus increasing the efficiency of H_2O_2 activation and thereby the oxidation of organic compounds. [35, 36] In addition, the combination of carboxylic acids (such as oxalic, malic, citric, tartaric acids, etc.) and iron (just dissolved or as oxides) can form ferricarboxylate complexes that absorb light irradiation with high quantum yield to trigger radical chain mechanisms of oxidation. [37-41] As a result, many of these ferricarboxylate complexes can be used to induce photodegradation of pollutants. Therefore, our investigations have been directed to the preparation of a citrate modified ferrihydrite. We hope the chelating ligands modification can enhance the adsorption capacity for heavy metal and some organic pollutants in water treatment procedures, since the adsorption reactions are closely related to the surface properties of the nanomaterials. On the other hand, we hope the synergistic effect between the photo-catalytic and heterogeneous Fenton reaction may further accelerate the degradation of organic pollutants.

In this article, flower-like citrate modified ferrihydrite microstructures (Fh1) were prepared by the simple oxidation and hydrolysis of ferric sulphate heptahydrate ($FeSO_4 \cdot 7H_2O$) in the presence of the citrate ions as the shape-directing/capping agent

at room temperature. Owing to the less expensive and nontoxic raw reaction materials, especially water as the solvent, our method represents an economic and green approach for the controlled synthesis of flower-like hierarchical ferrihydrite. Furthermore, the adsorption abilities and catalytic properties of as-obtained flower-like citrate modified ferrihydrite (Fh1) were studied. Compared with ferrihydrite (Fh2) prepared by mixing ferric and sodium hydroxide solutions ,[35] the as-obtained citrate modified ferrihydrite products(Fh1) exhibited a better adsorption ability to both MB and Cr(VI). In addition, Fh1 is employed in catalyzed oxidative decomposition of H_2O_2 for high concentration methylene blue (MB) dyes aqueous solution, exhibiting highly efficient heterogeneous catalytic activity for dyes decolorization. The presence of visible light resulted in additional efficient degradation of MB, which attributed to the reaction of hydroxyl radical photogenerated during the photoredox process taking place in Fe(III)–citrate upon irradiation.

2. Experimental section

2.1 Preparation of Ferrihydrite

All chemicals were of analytical reagent grade and used without further purification. The flower-like hierarchical ferrihydrite (Fh1) was prepared by the following procedure: 0.02 mol Fe(II) sulphate heptahydrate ($FeSO_4{\cdot}7H_2O$) and 0.02 mol citric acid was diluted with 100 mL distilled water at room temperature. NaOH solution (6.0 M) was added into the solution under stirring until pH 13. The suspension was magnetically stirred under constant aeration at a flow rate of 200 mL min^{-1} to ensure oxidation of the solid. The suspension was further stirred for 3 hours at room temperature. Finally, the resulting red products were centrifuged, washed with distilled water and ethanol before being dried at 60 ℃ for 24 h.

Ferrihydrite (Fh2) was synthesized according to the method described in our previous work.[35] Under vigorous magnetic stirring, 6 mol/L NaOH solution was added drop by drop to 50 mL of 1.0 mol/L ferric chloride solution. The rate of addition of the two solutions was controlled by maintaining pH 7 with an accuracy of better than 0.5 pH units. The above process was carried out under vigorous stirring at room temperature and the total volume was adjusted to 100 mL. The gels were collected, thoroughly washed with deionized water and dried in air at about 50 ℃.

2.2 Characterization

X-ray diffraction (XRD) patterns of the samples were recorded on a Bruker D8-ADVANCE X-ray diffractometer using Cu-K_α radiation at 40 kV and 40 mA. The compositions of the powders were characterized at room temperature by Fourier-transform IR spectroscopy on an FTIR-8900 instrument in the range 400-4000 cm^{-1}. Infrared spectra of the products were recorded by pelletizing a few milligrams of the sample with KBr. The morphologies of the samples were characterized by field-emission scanning electron microscopy (FESEM) (HITACHI S-4800). Selected area electron diffraction (SAED) and high-resolution TEM (HR-TEM) images of products were performed with a JEOL-2010 high resolution transmission electron microscopy (HRTEM, JEOL Ltd., Japan). Surface areas were determined by the BET method using N_2 adsorption-desorption isotherms. N_2 adsorption-desorption isotherms were measured on a gas sorption analyzer (Quantachrome, NOVA 4000e) at a liquid nitrogen temperature. XPS studies were performed on a Physical Electronics/PHI 5300 x-ray photoelectron spectrometer with the Al Ka X-ray source (hv 1486.6 eV). The position of the C1s peak was taken as a standard (with a banding energy of 284.8 eV).

2.3. Adsorption isotherm experiment

All the adsorption experiments were carried out in dark.

For the determination of the isotherms of methylene blue (MB) adsorption: The desired amounts of ferrihydrites in the suspension were mixed with the aqueous solutions of methylene blue. After stirring for 90 min, the samples were separated and the supernatant solutions were analyzed with a UV-Visible spectrophotometer (Yoke UV752) at a wavelength of 664 nm. To estimate the adsorption capacity, the initial concentrations of methylene blue were varied in the range of 20–50 mg L^{-1}, and the dosage of the ferrihydrites was kept at 0.3 g L^{-1}.

For the determination of the isotherms of heavy metal ions Cr(VI) adsorption: The solutions containing different concentrations of Cr(VI) (10, 20, 30, 40 and 50 mg L^{-1}) were prepared using $K_2Cr_2O_7$ as the source of heavy metal ion Cr(VI). 30 mg of the ferrihydrite was added to 20 mL of the above solution under stirring at room temperature. After stirring for 6 h, the solid and liquid were separated immediately and inductively coupled Atomic Absorption Spectrophotometer (Purkinje TAS-990) was used to measure the concentration of metal ions in the remaining solution.

2.4. (Photo-) Fenton-mediated and photocatalytic experiments

In a typical process, 30mg ferrihydrite was added to 100 mL 40 mg L^{-1} methylene blue (MB) solution and then magnetically stirred in the dark for 1.5 h to achieve the adsorption–desorption equilibrium between methylene blue (MB) and ferrihydrite, followed by the addition of 2 mL of hydrogen peroxide solution (H_2O_2, 30 wt %). The solution was then exposed to a 150 W tungsten-halogen lamp with a 420 nm cut off filter to provide visible-light irradiation. The reaction temperature was kept at room temperature by cooling water to prevent any thermal catalytic effect. The samples were collected by centrifugation every 30 min to measure methylene blue (MB) degradation by UV-vis spectroscopy (Yoke UV752).

2.5 Stability studies

Stability of the citrate modified ferrihydrite microstructures (Fh1) were examined by dispersing 0.07 g Fh1 in 20 mL different concentration of HCl or NaOH solution. After shaking for 3 h at 25 ℃, the leached iron concentration were analyzed by using a UV-vis spectroscopy (Yoke UV752), according to the 5-sulfosalicylic acid (SSA) method. [42]

3. Results and discussions

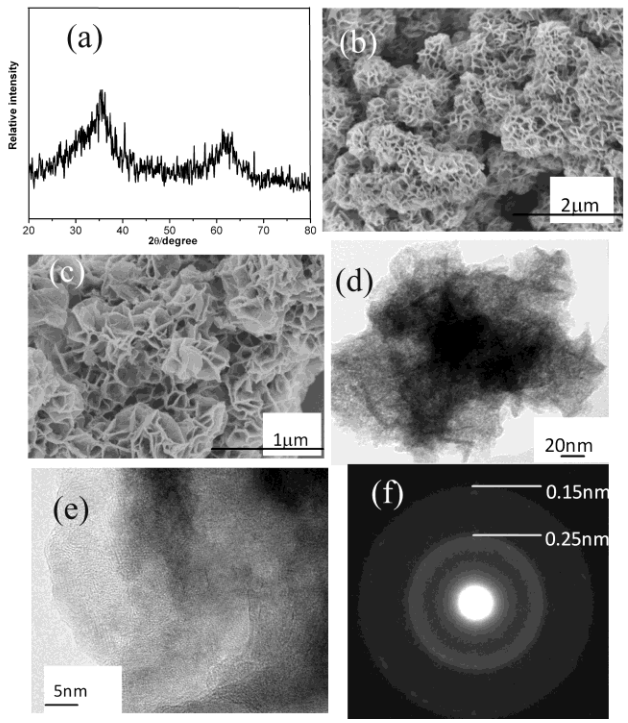

Fig.1 (a) X-ray diffraction (b) low magnification SEM image (c) high-magnified SEM image (d) TEM image (e) HRTEM image (f) SAED patterns of the product Fh1 obtained in a typical synthesis.

Fig. 1a shows the XRD pattern recorded for the sample. Two broad peaks are found at 2θ~ 35° and 2θ~ 63°, respectively. This X-ray diffraction pattern is consistent with the previous reports of pure 2-line ferrihydrite. [43] Fig. 1b is the low-magnification FESEM image of the as-synthesized product, which clearly demonstrates that the products are composed of numerous flower-like aggregates, which arranged compactly because of the conglomeration. The TEM image of the flower-like microstructures (Fig. 1d) clearly demonstrates that the microstructures are composed of close-packed thin nanosheets, which agrees with the HRSEM result (Fig. 1c). Fig. 1e shows HRTEM images of the edges of 2-line ferrihydrite aggregates. Widely scattered areas that have distinct lattice fringes are surrounded by areas without recognizable fringes. Although nanodiffraction shows that the sample contains some near-amorphous material, areas without lattice fringes in HRTEM images can also be produced by crystallites that are not in appropriate orientations or are superposed on each other. The electron diffraction pattern of 2-line ferrihydrite shows two rings corresponding to interplanar distances of 0.15 and 0.25 nm (Fig. 1f). The measured d-spacings, typical of 2-lines ferrihydrite, are in agreement with those calculated by X-ray diffraction.

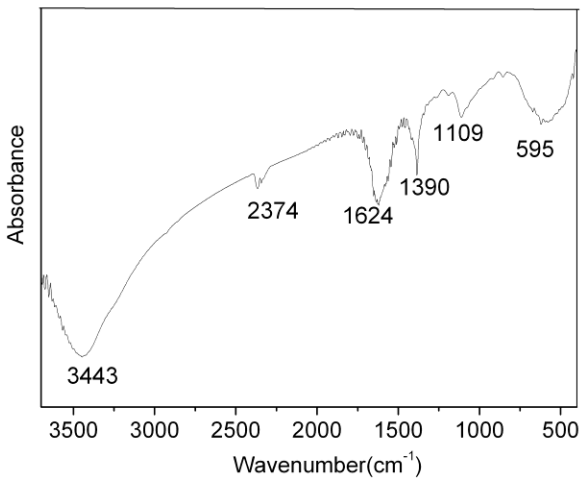

Fig. 2 FTIR spectra of the product Fh1 obtained in a typical synthesis.

To verify the adsorption and coordination of citrate to Fe(Ⅲ) , FTIR absorption of the product was measured. Fig. 2 shows the FT-IR spectra of flower-like ferrihydrite. The band at 3443 cm^{-1} can be assigned to the stretching mode of H_2O molecules. A very strong and broad band with peaks at 595 cm^{-1} are typical for low crystalline ferrihydrite or "amorphous" iron(III)-hydroxide. The band at 1624 cm^{-1} and 1390 cm^{-1} correspond to asymmetric and symmetric stretching of COO^- groups, which proved the presence of the citrate ions in the sample. The citrate anion is coordinated

to the metal ions through both of its two COO^- groups and its C–OH group. This statement is supported by the split of the band of free acid carboxylic groups (≈1730 cm^{-1}) into two very strong bands characteristic for coordinated carboxylic groups ($\nu_{OCOasym}$= 1624 cm^{-1} and ν_{OCOsym}=1390 cm^{-1}) and by the shift towards lower frequencies (1120 cm^{-1}→ 1109 cm^{-1}) of the band assigned to ν(C–OH).

Fig. 3 shows the N_2 adsorption-desorption isotherm and pore size distribution curve (inset in Fig. 3) of the flower-like citrate modified ferrihydrite (Fh1). The isotherm can be classified as type IV with an apparent hysteresis loop in the range 0.5–1.0 P/P_0, indicating the presence of mesopores. The plot of pore size distribution determined by the Barrett–Joyner–Halenda (BJH) method shows that these flower-like ferrihydrite has pores with diameters of ca. 18 nm (inset in Fig. 3) and that the BET surface area is 276.2 m^2/g, which is larger than that of previous reports (133 m^2/g). [44]

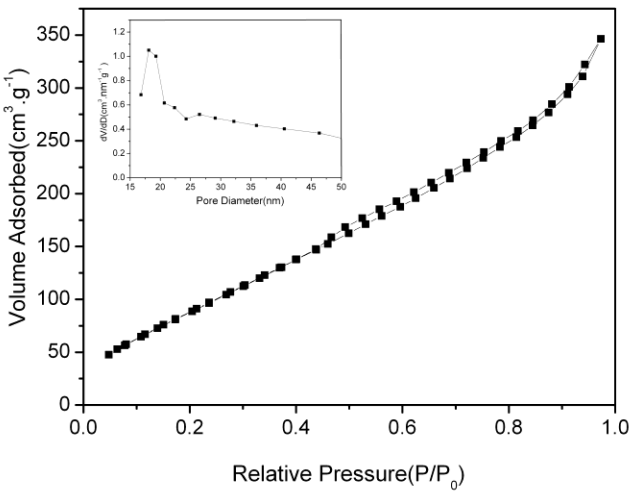

Fig. 3 The nitrogen adsorption-desorption isotherm and pore size distribution curve (inset) of Fh1 obtained in a typical synthesis.

XPS analysis was conducted to investigate the oxidation state of Fe on the surface of citrate modified ferrihydrite (Fh1). Fig. 4 shows the narrow region spectra for Fe 2p3/2 which were composed of four peaks at 709.5, 710.4, 711.5 and 713.0 eV, respectively. The peak located at 711.5 eV corresponds unambiguously to oxygen-bonded ferric ion (Fe(III)–O). The peak arising at 709.5 eV can be assigned to Fe(II)–O, [45] which indicate existence of Fe(II) ions on the surface of citrate modified ferrihydrite (Fh1).

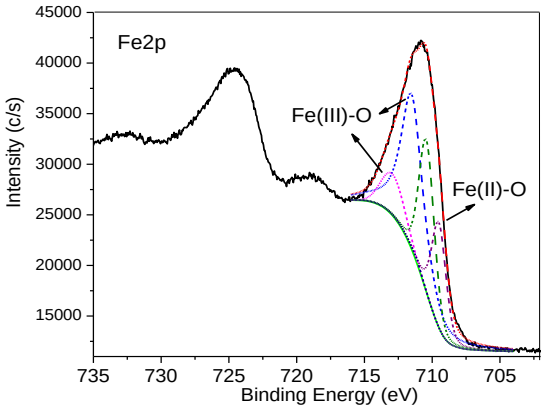

Fig. 4 XPS spectra for the narrow scan of Fe 2p on the surface of citrate modified ferrihydrite (Fh1)

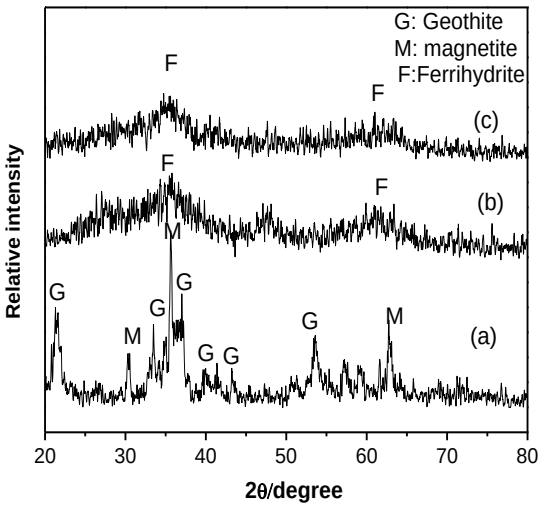

Fig. 5 X-ray diffraction of the samples obtained for 6 h with the addition of citrate: (a) 0, (b) 0.05, (c) 0.10 mol L^{-1}.

To investigate the effect of the citrate on the formation of flower-like ferrihydrite (Fh1), a series of comparative experiments were carried out. The experiments showed that citrate ions played key roles in the formation of the ferrihydrite complex microstructures. In the absence of citrate, the obtained product is made of the mixture of geothite (α-FeOOH) and magnetite (Fe_3O_4) crystals according to the XRD analysis (Fig. 5a). The SEM image (Fig. 6a) shows that the crystals are mainly rod-like particles. At a low concentration of citrate ions (0.05 mol L^{-1}), the products are irregular shape aggregations consist of quasi-spherical nanoparticles as shown in Figure 6b. If the concentration of citrate increases to 0.10 mol L^{-1}, the products are flower-like aggregations composed of plate-like nanoparticles (shown in Fig. 6c). As the citrate concentration further increases to 0.20 mol L^{-1}, the samples are composed of subunits with more prominent

sheet-like structure (shown in Fig. 6d). It is obvious that the sizes of the petals in the flowerlike microstructures grow gradually with the increasing of the citrate ions concentration. The corresponding XRD patterns of samples (Fig. 5b, 5c and 1a) indicate that they are also single-phase ferrihydrites.

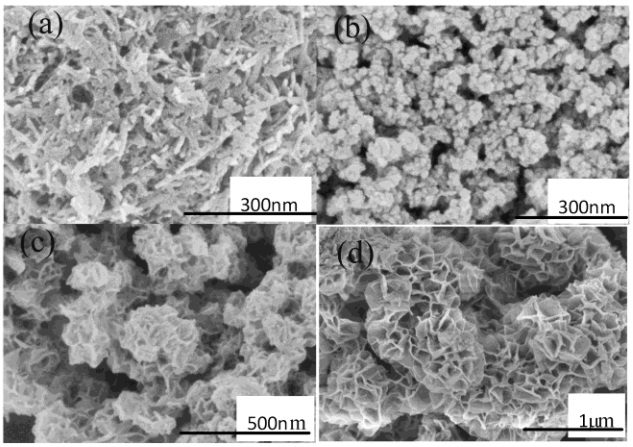

Fig. 6 FE-SEM images of the samples obtained for 6 h with the addition of citrate: (a) 0, (b) 0.05, (c) 0.10, (d) 0.20 mol L^{-1}.

Time-dependent experiments were carried out to understand the formation process of such interesting hierarchical flower-like ferrihydrite. Fig. 7 shows the SEM images of the samples obtained with different reaction durations. As can be seen in Fig. 7a, at the early stage of the reaction (0.5 h), the nanoparticles combined with each other and self-assembled into undeveloped flower-like superstructures. When the reaction duration was increased to 1 h, the building blocks of the superstructures transformed into nanosheets and the flower-like architectures formed (Fig. 7b). As the reaction time was further increased, well-structured flower-like architectures were obtained and the sizes of the nanosheets in the flower-like hierarchical microstructures grew bigger and bigger (Fig.7c, Fig.7d).

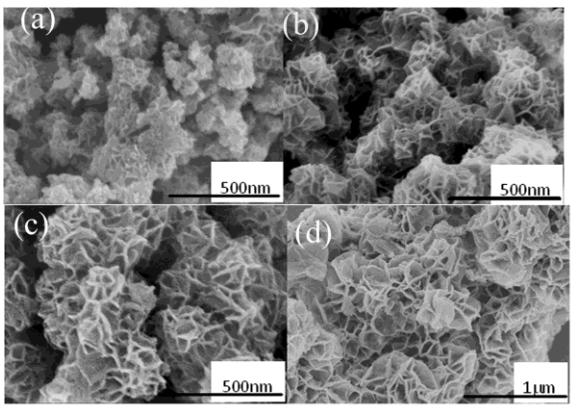

Fig. 7 The morphology evolution of the samples prepared at different reaction times: (a) 0.5 h, (b) 1 h, (c) 2 h, (d) 4 h. ($FeSO_4$: 0.20 mol L^{-1}, citrate: 0.20 mol L^{-1}).

Based on the above experimental observations, a plausible formation mechanism of the hierarchical flower-like ferrihydrite is proposed. Initially, OH^- ions reacted with the available Fe^{2+} and O_2 to form the ferrihydrite primary nanocrystal nuclei. Then, the primary ferrihydrite particles aggregated into irregular shape agglomerations through oriented aggregation to greatly reduce the interfacial energy of small primary nanocrystals. In the subsequent process, the building blocks of the superstructures further grow into larger nanosheets driven by the minimization of surface energy and form the fully developed flower-like ferrihydrite architectures. On the basis of the literature and the investigations described above, we believe that citrate plays two major roles in our system. On the one hand, ferrous ions coordinate with citrate molecules to form Fe(II)-citrate complexes, which decreases the free Fe^{2+} concentration in solution and results in the slow generation of ferrihydrite nanoparticles. On the other hand, citrate can also serve as a shape modifier and controller, which may bind to certain crystal faces of the ferrihydrite particles through its COO^- and -OH functions. This surface interaction can inhibit ferrihydrite crystals elongated perpendicular to these planes, resulting in the formation of ferrihydrite nanosheets. Further works are underway to investigate the detail formation of the flower-like ferrihydrite architectures.

Because of their novel 3D hierarchical porous structure and citrate modification, we expected that these flower-like citrate modified ferrihydrite (Fh1) from our experiment would be useful in water treatment. Methylene blue (MB), a dye commonly used in the textile industry, was chosen as a model organic water pollutant. We also investigated the removal ability of ferrihydrite synthesized according to the method described in our previous work (Fh2) under the same experimental conditions. These two kinds of ferrihydrites were used to remove the methylene blue (MB) dye solution (20 mg/L) in dark. It was found that the as-prepared flower-like ferrihydrite (Fh1) showed much better removal ability than ferrihydrite (Fh2). Within 80 min, about 95.1% of MB solution can be adsorbed by Fh1. When Fh2 is employed as adsorbent, this value is 59.3% (Fig. 8) .

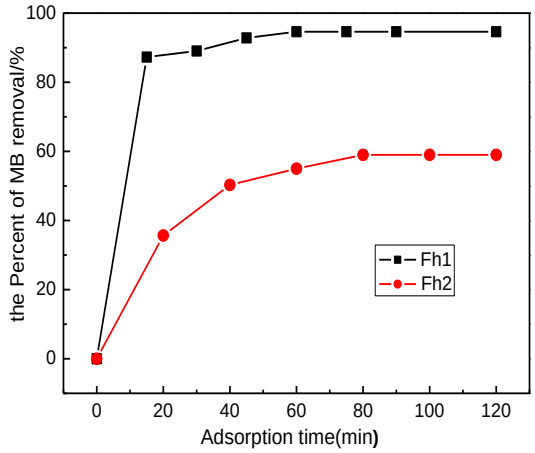

Fig. 8 Adsorption kinetics of MB removal with Fh1 and Fh2. Conditions: ambient temperature, pH 7 and 0.03 g adsorbent, The initial concentration of MB is 20 mg/L

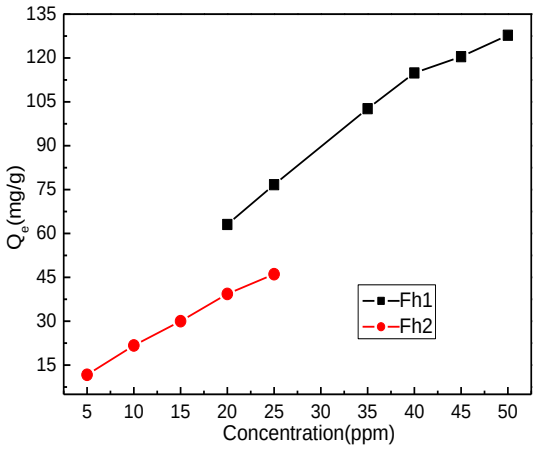

Fig. 9 Adsorption isotherm of Methylene blue on Fh1 and Fh2. Conditions: ambient temperature, pH 7 and 0.03 g adsorbent

Adsorption isotherms of MB with different initial concentrations for 90 min of adsorption are illustrated in Fig. 9. It is clear that the adsorption amount increases with increasing of initial concentration of MB solution. The adsorption equilibrium data obtained for the Fh1 and Fh2 were fitted using Langmuir and Freundlich isotherm models (Fig. 10). The Langmuir adsorption model is used to calculate the maximal adsorption capacity: $Q_e = Q_m bC_e/(1+bC_e)$, where Q_e (mg g^{-1}) is the amount of adsorbed ions at equilibrium, C_e (mg L^{-1}) is the equilibrium solute concentration, Q_m(mg g^{-1}) is the maximal adsorption capacity at complete monolayer coverage and b is the equilibrium constant (L mg^{-1}). The Freundlich isotherm describes reversible adsorption onto heterogeneous surfaces and is not restricted to the formation of the monolayer of adsorbate. The Freundlich isotherm is expressed as: $Q_e = K_F C_e^{1/n}$, where K_F and n are the Freundlich constants. Table 1 lists the fitted results of Langmuir and Frieundlich models for the methylene blue (MB) adsorption data by the samples. The Langmuir maximum adsorption capacity (Q_{max}) for methylene blue (MB) by Fh1 (139.86 mg/g) is significantly higher than that by Fh2 (76.34 mg/g). The Freundlich adsorption capacity constants (K_F) of the samples shows the order of Fh1 > Fh2, which is in agreement with the Langmuir adsorption capacity (Q_{max}). The correlation coefficients of Langmuir model for the methylene blue (MB) adsorption data by both Fh1 and Fh2 are high (R^2 = 0.997). The Freundlich correlation coefficient is relatively low for the adsorption data by Fh1 (R^2 = 0.967) and high for the adsorption data by Fh2 (R^2 = 0.998).

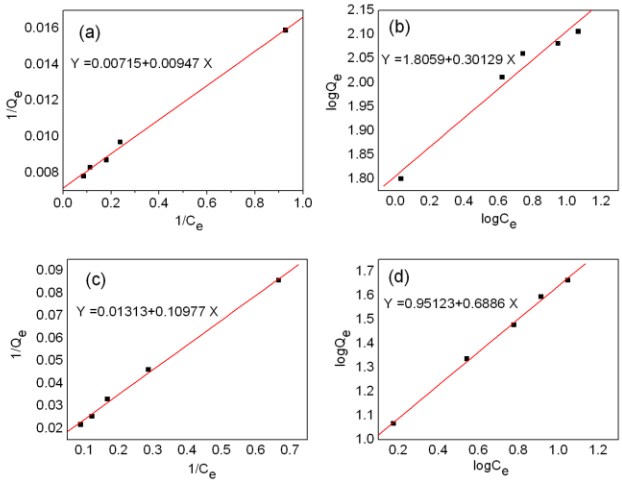

Fig.10 (a) Langmuir adsorption isotherm, (b) Freundlich adsorption isotherm for adsorption of Methylene blue by Fh1, (c) Langmuir adsorption isotherm, (d) Freundlich adsorption isotherm for adsorption of Methylene blue by Fh2.

To further verify the advantage of the hierarchical flower-like Fh1 in water treatment, we evaluate the adsorption capabilities for toxic heavy metal ion Cr(V) at room temperature in dark. These two kinds of ferrihydrites were used to adsorb the Cr(VI) solution (30 mg/L). It was found that the as-prepared flower-like Fh1 showed much better removal ability than Fh2. Within 5 h, about 78.4% of Cr(VI) solution can be adsorbed by Fh1. When Fh2 is employed as adsorbent, this value is 42.1% (Fig. 11). Adsorption isotherms of Cr(VI) with different initial concentrations for 6h of adsorption are illustrated in Fig. 12. It is shown that the adsorption amount increases with increasing of initial concentration of Cr(VI). The adsorption equilibrium data obtained for the Fh1 and Fh2 were fitted using Langmuir and Freundlich isotherm models (Fig. 13). Table 1 lists the fitted

results of Langmuir and Frieundlich models for the Cr(VI) adsorption data by the samples. The Langmuir maximum adsorption capacity (Q_{max}) for Cr(VI) by Fh1 (19.569 mg/g) is significantly higher than that by Fh2 (12.285 mg/g). The Freundlich adsorption capacity constants (K_F) of the samples shows the order of Fh1 > Fh2, which is in agreement with the Langmuir adsorption capacity (Q_{max}). The correlation coefficients of Langmuir model for the Cr(VI) adsorption data by both Fh1 and Fh2 are high (R^2 = 0.992 and 0.993, respectively). The Freundlich correlation coefficient is relatively low for the adsorption data by Fh1 (R^2 = 0.911) and high for the adsorption data by Fh2 (R^2 = 0.991).

Table 1. Langmuir and Freundlich isotherm constants for the adsorption of Methylene blue (MB) and Cr(VI) onto different adsorbents.

Adsorb-ate	Adsorbent	Langmuir model $Q_e = Q_m b C_e/(1+bC_e)$			Freundlich model $Q_e = K_F C_e^{1/n}$		
		Q_{max} (mg/g)	b	R^2	K_F	n	R^2
MB	Fh1	139.86	0.755	0.997	63.973	3.322	0.967
	Fh2	76.34	0.119	0.997	8.933	1.452	0.998
Cr(VI)	Fh1	19.569	0.437	0.992	6.714	2.857	0.911
	Fh2	12.285	0.137	0.993	2.472	2.364	0.991

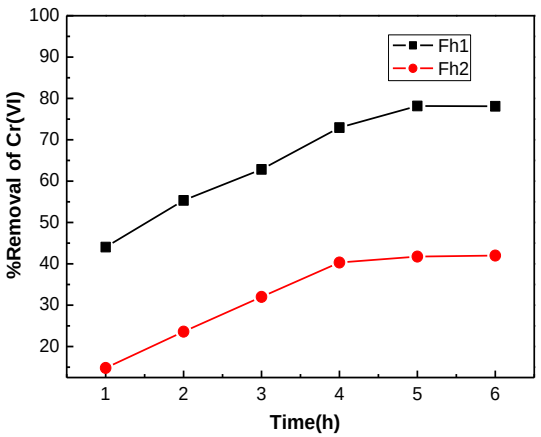

Fig. 11 Adsorption kinetics of Cr(V) removal with Fh1 and Fh2. Conditions: ambient temperature, pH 2.5, 0.03 g adsorbent, initial concentration of Cr(VI) is 30 mg/L.

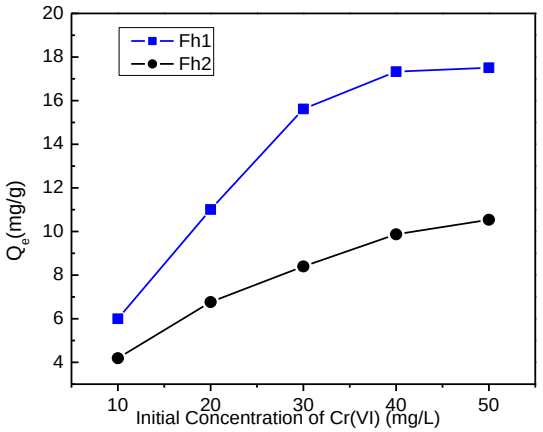

Fig. 12 Adsorption isotherm of Cr(V) on Fh1 and Fh2 Conditions: ambient temperature, pH 2.5, 0.03 g adsorbent, initial concentration of Cr(VI) is 30 mg/L.

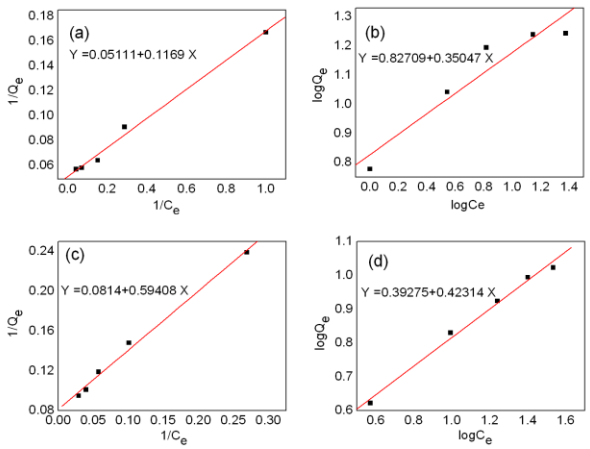

Fig. 13 (a) Langmuir adsorption isotherm (b) Freundlich adsorption isotherm for adsorption of Cr(IV) ions by Fh1, (c) Langmuir adsorption isotherm (d) Freundlich adsorption isotherm for adsorption of Cr(IV) ions by Fh2.

It is clear that the as-prepared ferrihydrite with the flower-like structure (Fh1) exhibits much better removal capacities for methylene blue (MB) and Cr(VI) than the ferrihydrite (Fh2). It is known that the adsorption capacity of a material is determined by its porous structure, chemical structure, and active sites on its surface. Obviously, the specific surface areas of the as-obtained the flower-like structure ferrihydrite (Fh1)(276.2 m^2/g) are far higher than that of the ferrihydrite (Fh2) (176.6 m^2/g). For Fh1, the micrometer-size overall structure is composed of many ultra-thin nanosheets. This hierarchical nanostructure can provide facile mass transportation, avoid aggregation and maintain high surface area, which ensure the high density of surface active adsorption sites. The better performance for methylene blue (MB)

and Cr(VI) removal can be attributed to their high specific surface areas and novel structures of their surfaces. On the other hand, the adsorption of heavy metal and organic contaminants took place via surface exchange reactions until the surface functional sites are fully occupied, and thereafter contaminants could diffuse into adsorbent for further interactions with functional groups. Thus, the citrate modification of ferrihydrite is essential to enhance the target adsorption capability. Many researches showed that iron oxides are efficient adsorbents for anionic and organic pollutants. However, the adsorption capacity for metal cations by iron oxides is relatively low due to the electrostatic repulsion. The citrate modified ferrihydrite microstructures (Fh1) have a high affinity with heavy-metal cations because they possess surfaces with negative charge and carboxylate anions.

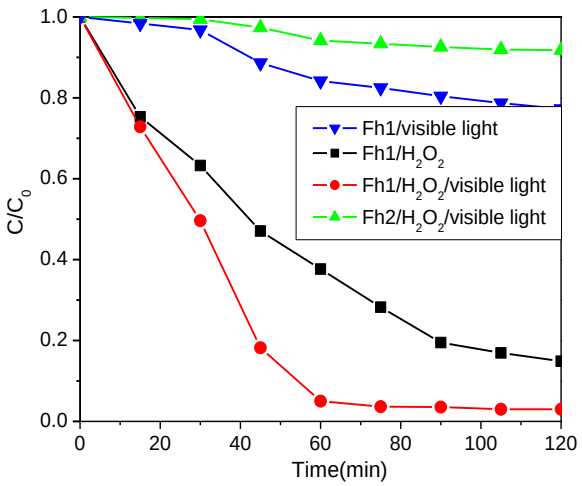

Fig.14 The time-dependent photo-degradation of MB under different situations.

The catalytic activity of the as-prepared samples was evaluated for MB degradation under visible light illumination in the presence of H_2O_2. It indicates that the simultaneous presence of citrate modified ferrihydrite nanoparticles (Fh1) and H_2O_2 degraded 99.7% of MB within 120 min under visible light. Additionally, an experiment was also performed in the presence of ferrihydrite (Fh2) with H_2O_2 under visible-light illumination (Fig. 14). It should be noted that the degradation efficiency of MB was only 8.3%. These experimental results indicate that Fh1 exhibited better catalytic activity than Fh2 in the degradation of MB aqueous solution in the presence of H_2O_2 under visible-light irradiation. The modification of citrate played an important role in the catalytic activity of ferrihydrite.

To determine whether the degradation is due to photocatalytic or Fenton-like reactions, the time-dependent degradation of MB under different situations are plotted and shown in Fig. 14. As shown in Fig. 14, in the absence of H_2O_2 (only MB and ferrihydrite Fh1), 22.1% of MB has been degraded after visible-light irradiation for 120 min. It indicates that citrate modified ferrihydrite Fh1 exhibit better visible-light photocatalyic activity for MB degradation than Fh2 (ferrihydrite without citrate modification) under visible-light illumination at neutral pH. It has been previously revealed that Fe(III)-citrate complexes can undergo ligand-to-metal charge transfer (LMCT) process and the subsequent oxygen-related radicals cycling to generate Fe(II) and reactive oxygen species such as $HO_2\bullet$ /$O_2\bullet^-$, H_2O_2 and •OH. As a result, degradation efficiency of MB employing the Fh1/ visible-light system was higher than the Fh2/ visible-light system. Main photochemical reactions of the Fe(III)-citrate complex are listed as follows [46]:

$$Fe(III)\text{–}Cit + h\nu \rightarrow Fe(II) + \bullet OOC\text{–}C(OH)(CH_2COO)_2^{2-} \quad (1)$$

$$\bullet OOC\text{–}C(OH)(CH_2COO)_2^{2-} \rightarrow \bullet C(OH)(CH_2COO)_2^{2-} + CO_2 \quad (2)$$

$$\bullet C(OH)(CH_2COO)_2^{2-} + O_2 \rightarrow CO(CH_2COO)_2^{2-} + HO_2\bullet \quad (3)$$

$$HO_2\bullet \rightarrow O_2\bullet^- + H^+ \quad (4)$$

$$O_2^{-}\bullet + Fe(II) + 2H^+ \rightarrow Fe(III) + H_2O_2 \quad (5)$$

$$HO_2\bullet + Fe(II) + H^+ \rightarrow Fe(III) + H_2O_2 \quad (6)$$

$$Fe(II) + H_2O_2 \rightarrow Fe(III) + \bullet OH + OH^- \quad (7)$$

When H_2O_2 is added, the degradation of the organic pollutants is significantly accelerated, and the removal radio of MB increased from 22.1% to 99.7% within 120 min under visible-light illumination, indicating the samples have Fenton-like catalytic activity. To further determine whether the visible-light play an important role in the degradation process, the control experiment in the dark is carried out. In the Fh1/ H_2O_2 system, significant decolorization of MB (88.1%) was observed in the dark. It was reported the presence of iron (II) ions in the Fe-bearing minerals can enhance the production rate of HO•, and enhance the efficiency of Fenton-like catalytic properties. [47-50] The fact that Fh1was capable of degrading MB in the dark can be attributed to the presence of adsorbed Fe(II), which could catalyze the Fenton-like reaction. The Fe(II) ions were originated from the reactant $FeSO_4$ because the modified chelating ligands citrate can enhance the Fh1 adsorption capacity for Fe(II) ions. As mentioned above, the simultaneous presence of citrate modified ferrihydrite (Fh1), H_2O_2 and visible-light provides the most effective conditions for the degradation of methylene blue (MB). The concurrence of the

Fenton-like process catalyzed by adsorbed Fe(II) and the photochemical reactions of the Fe(III)-citrate complex results in the formation of serials of radicals including hydroxyl radicals, and then the target substrates are decomposed.

The citrate modified ferrihydrite microstructures (Fh1) were exposed to different concentrations of HCl or NaOH for 3 h. The leached Fe content of the Fh1 was determined. No significant Fe leaching was observed in acid with concentration range of 10^{-4} ~10^{-2} mol L^{-1} or alkali solution with concentration range of 0.5~1 mol L^{-1} (Table 2). It is more stable in alkaline environment compared to acidic environment. Furthermore, Fh1 could be preserved for five months at room temperature without deterioration, which indicating the good stability of citrate modified ferrihydrite microstructure.

Table 2. Leached Fe rate of Fh1 after treated by different concentrations HCl and NaOH solution.

	HCl(mol/L)						NaOH (mol/L)	
Concentration	10^{-4}	10^{-3}	10^{-2}	0.1	1	2	0.5	1
Leaching rate (%)	3.69	4.36	4.68	15.8	85.6	100	0.29	0.18

4. Conclusions

In conclusion, we have used $FeSO_4 \cdot 7H_2O$, a nontoxic and inexpensive reagent to synthesize flower-like citrate modified ferrihydrite microstructures (Fh1) by a simple chemical route. Citrate ions have been introduced as shape modifiers and proved to be efficient to control the shape of the ferrihydrite microstructures. The reaction mechanism and the self-assembly evolution process were studied. The surface properties and adsorption ability of the as-prepared ferrihydrite (Fh1) were significantly influenced by the modification of citrate ions. As a result, the as-obtained citrate modified ferrihydrite (Fh1) exhibit larger adsorption capacity towards methylene blue (MB) and heavy metal ions Cr(VI) than the ferrihydrite (Fh2) without modified citrate. In addition, the as-prepared ferrihydrite (Fh1) exhibited high activity to produce hydroxyl radicals through catalytic decomposition of H_2O_2 and can degrading highly concentrated MB solution. The presence of iron (II) ions on the surface of citrate modified ferrihydrite (Fh1) enhances its Fenton-like catalytic performance. At the same time, iron oxides and citrate ions can set up a photo-Fenton-like system and potentially use visible-light as the irradiation source to produce reactive species, which would play an important role in the oxidation of organic materials. These results indicate that Fh1 has potential applications in adsorption and visible-light photo-catalysis for environmental remediation.

Acknowledgments

We greatly appreciate the support of the National Natural Science Foundation of China (No. 21277040, 21272054, 21072043 and 21203052), the Youth Foundation of Hebei provincial department of education (No. 2010142), Nature Science Foundation of Hebei Province (B2010000362), the Key Project of Chinese Ministry of Education(No207012) and the Scientific Research Foundation for the Returned Overseas Chinese Scholars, State Education Ministry.

Notes and references

[a] *College of Chemistry and Materials Science, Hebei Normal University , Shijiazhuang , 050024, China*
[b] *Institute of Coal Chemistry, Chinese Academy of Sciences, Taiyuan, 030001*
[c] *Key Laboratory of Inorganic Nanomaterial of Hebei Province, Shijiazhuang 050024,China. Fax: +86-311-8078-7400; Tel: 86-311-8078-7400; E-mail: weiyu@mail.hebtu.edu.cn; weiyuhebtu@163.com*

1 I. Carabante, M. Grahn, A. Holmgren, J. Kumpiene and J. Hedlund, *Colloids Surf A: Physicochem. Eng. Aspects*, 2009, **346(1–3)**, 106-113.
2 P. Xu, G. M. Zeng, D. L. Huang, C. L. Feng, S. Hu, M. H. Zhao, C. Lai, Z. Wei, C. Huang, G. X. Xie and Z. F. Liu, *Sci Total Environ.*, 2012, **424**, 1-10.
3 J. M. Gu, S. H. Li, E. B. Wang, Q. Y. Li, G. Y. Sun, R. Xu and H. Zhang, *J. Solid State Chem.*, 2009, **182** , 1265-1272.
4 S. W. Cao and Y. J. Zhu, *J. Phys. Chem. C*, 2008, **112** , 6253-6257.
5 P. Zhang, Z. P. Guo, and H. I. Liu, *Electrochim. Acta*, 2010, **55**, 8521-8526.
6 F. H. Zhang, H. Q. Yang and X. L. Xie, *Sens. Actuators, B*, 2009, **141**, 381-389.
7 J. B. Lian, X. C. Duan, J. M. Ma, P. Peng, T. Kim and W. Zheng, *ACS Nano.* , 2009, **3**, 3749-3761.
8 J. B. Fei, Y. Cui, J. Zhao, L. Gao, Y. Yang and J. B. Li, *J. Mater. Chem.*, 2011, **21**, 11742-11746.
9 L. S. Zhong, J. S. Hu, H. P. Liang, A. M. Cao, W. G. Song and L. J. Wan, *Adv. Mater.*, 2006, **18**, 2426-2431.
10 S. W. Cao and Y. J. Zhu, *Acta Mater.*, 2009, **57(7):** 2154-2165.
11 L. H. Ai, C. Y. Zhang and Z. L. Chen, *J. Hazard. Mater.*, 2011, **3**, 1515-1524.
12 X. H. Liu, J. J. Guo, Y. H. Cheng, Y. Li, G. J. Xu and P. Cui, *J. Cryst. Growth*, 2008, **311**, 147-151.
13 A. K. Ganguli and T. Ahmad**,** *J. Nanosci. Nanotechno.*, 2007, **7**, 2029-2035.
14 H. Li, W. Li, Y. J. Zhang, T. S. Wang, B. Wang, W. Xu, L. Jiang, W. G. Song, C. Y. Shu and C. R. Wang, *J. Mater. Chem.*, 2011, **21**, 7878-7881.
15 J. Hu, G. Chen and I. Lo, *Water Res.*, 2005, **39(18)**, 4528-4536.

16 J. Hu, M. Lo and G. Chen, *Sep. Purif. Technol* ., 2007, **58(1)**, 76-82.

17 J. Hu, L. Zhong, W. Song and L. Wan, *Adv. Mater*., 2008, **20**, 2977-2982.

18 N. N. Nassar, *J. Hazard. Mater.*, 2010, **184**, 538-546.

19 S. W. Cao, Y. J. Zhu and G. F. Cheng, *J. Phys. Chem. Solids*, 2010, **71(12),** 1680-1683.

20 G. Liu, Q. Deng, H. Q. Wang, H. L. Ng Dickon, M. G. Kong, W. P. Cai and G. Z. Wang, *J. Mater. Chem.*, 2012, **22**, 9704-9713.

21 L. L. Li, Y. Chu, Y. Liu and L. Dong, *J. Phys. Chem. C*, 2007, **111:** 2123-2127.

22 S. Y. Lian, E. B. Wang, L. Gao, D. Wu, Y. L. Song and L. Xu, *Mater. Res. Bull*., 2006, **41:** 1192-1198.

23 S. W. Cao and Y. J. Zhu, *Nanoscale Res. Lett.*, 2011, **6(1)**, 1.

24 J. R. Huang, M. Yang , C. P. Gu , M. H. Zhai , Y. F. Sun and J. H. Liu, *Mater. Res. Bull*., 2011, **46**, 1211-1218.

25 S. Y. Zeng, K. B. Tang, T. W. Li, Z. Liang, D.Wang, Y. Wang,Y. Qi and W. Zhou, *J. Phys. Chem. C*, 2008, **112**, 4836-4843.

26 L. P. Zhu, N. C. Bing, L. L. Wang, H. Y. Jin, G. H. Liao and L. J. Wang, *Dalton Trans*., 2012, **41**, 2959-2965.

27 S. W. Cao and Y. J. Zhu, *J. Phys. Chem. C*, 2008, **112(16):** 6253-6257.

28 I. Jessica, J. Nieto and K. Tamar, *Photochem. Photobiol. Sci.*, 2013, **12**, 1596-1605.

29 E. Rodriguez, G. Fernandez, B. Ledesma, P. Alvarez and F. J. Beltran, *Appl. Catal., B: Environ*., 2009, **92**, 240-249.

30 R. Matta, K. Hanna and S. Chiron, *Sci. Total Environ.*, 2007, **385**, 242-251.

31 H. H. Huang, M. C. Lu and J. N. Chen, *Water Res*., 2001, **35**, 2291-2299.

32 J. C. Barreiro, M. D. Capelato, N. L. Martin and H. C. B. Hansen, *Water Res*., 2007, **41(1)**: 55-62.

33 M. Hartmann, S. Kullmann and H. Keller, *J. Mater. Chem.*, 2010, **20**, 9002-9017.

34 P. V. Nidheesh, R. Gandhimathi, S. Velmathi and N. S. Sanjini, *RSC Adv.*, 2014, **4**, 5698-5708.

35 H. Liu, Y. Wang, Y. Ma, Y. Wei and G. Pan, *Chemosphere*, 2010, **79**, 802-806.

36 Y. Wang, Y. Zhao, Y. Ma, H. Liu and Y. Wei, *J. Mol. Catal. A-Chem*., 2010, **325**, 79-83.

37 F. Li, J. Chen, .i Liu, J. Dong, T. Liu, *Biol Fertil Soils*, 2006, **42**: 409-417.

38 J. Lei, C. Liu, F. Li, X. Li, S. Zhou, T. Liu, M. Gu and Q. Wu, *J. Hazard. Mater.*, 2006, **137**, 1016-1024.

39 C. Zhang, L. Wang, F. Wu and N. Deng, *Environ. Sci. Pollut. Res.*, 2005, **13**, 156-160.

40 H. B. Abrahamson, A. B. Rezvani, and J. G. Brushmiller, *Inorganica Chimica Act*., 1994, **226**, 117-127.

41 X. Ou, X. Quan, S. Chen, F. Zhang, and Y. Zhao, *J. Photoch. Photobio. A*, 2008, **197**, 382-388.

42 D. Karamanev, L. Nikolov and V. Mamatarkova, *Miner. Eng.*, 2002, **15(5)**: 341-346.

43 F. M. Michel, L. Ehm, S. M. Antao, P. L. Lee, P. J. Chupas, G. Liu, D. R. Strongin, M. A. A. Schoonen, B. L. Phillips and J. B. Parise, *Science*, 2007, **316**, 1726-1729.

44 Z. Li, T. Zhang and K. Li, *Dalton Trans.*, 2011, **40**, 2062-2066.

45 Y. Lee, W. Lee, *J. Hazard. Mater.*, 2010, **178**, 187-193.

46 O. Abida, M. Kolar, J. Jirkovsky and G. Mailhot, *Photochem. Photobiol. Sci.*, 2012, **11**, 794-802.

47 S. S. Lin and M. D. Gurol, *Environ. Sci. Technol.*, 1998, **32,** 1417-1423.

48 R. Matta, K. Hanna and S. Chiron, *Sep. Purif. Technol*., 2008, **61**,442-446.

49 R. Matta, K. Hanna, T. Kone and S. Chiron, *Chem. Eng. J.*, 2008, **144**, 453-458.

50 X. Xue, K. Hanna and N. Deng, *J. Hazard. Mater.*, 2009, **166**, 407-414.